Journal of Engineering Science and Technology
Vol. 12, No. 2 (2017) 388 - 404


# MAXIMUM AIR SUCTION INTO HORIZONTAL OPEN ENDED CYLINDRICAL LOUVERED PIPE

SAMEER RANJAN SAHU, DIPTI PRASAD MISHRA*

Department of Mechanical Engineering,
Birla Institute of Technology, Mesra, Ranchi, 835215, India
*Corresponding Author: dpmishra@bitmesra.ac.in

**Abstract**

The main approach behind the present numerical investigation is to estimate the mass flow rate of air sucked into a horizontal open-ended louvered pipe from the surrounding atmosphere. The present numerical investigation has been performed by solving the conservation equations for mass, momentum and energy along with two equation based $k$-$\varepsilon$ model for a louvered horizontal cylindrical pipe by finite volume method. It has been found from the numerical investigation that mass suction rate of air into the pipe increases with increase in louvered opening area and the number of nozzles used. Keeping other parameters fixed, for a given mass flow rate there exists an optimum protrusion of nozzle for highest mass suction into the pipe. It was also found from the numerical investigation that increasing the pipe diameter the suction mass flow rate of air was increased.

Keywords: Louvers, Entrainment, Nozzle, Exhaust gas, Horizontal pipe

## 1. Introduction

The temperature of the hot exhaust gases released from the vehicles is about 70 $^{o}$C, Petter Kirloskar (Diesel CI Engine) 10hp 1500 rpm, twin cylinder vertical 4 stroke, compression ratio 16.5:1, bore 0.08 m, stroke 0.11 m, exhaust pipe diameter 0.05 m which are released directly into the atmosphere. These hot gases give rise to many environmental problems as well as respiratory diseases. Due to direct release of hot exhaust gases, the local environmental temperature is rising every day, causing adverse climatic changes thereby making it difficult for every organism to survive on the planet. These problems are very acute in metro cities in rush hours when the vehicles are temporarily stopped at the crossings due to

## Nomenclatures

| | |
|---|---|
| $A_h$ | Louvers opening area, $m^2$ |
| $A_{pf}$ | Area of the entrance face of the pipe, $m^2$ |
| $C_{1\varepsilon}$ | Constant of value 1.44 |
| $C_{2\varepsilon}$ | Constant of value 1.92 |
| $D_{CD}$ | Diameter of computational domain, m |
| $D_h$ | Diameter of circular louver, m |
| $D_n$ | Diameter of nozzle, m |
| $D_P$ | Diameter of pipe, m |
| $D_{pd}$ | Pitch circle diameter, m |
| $D_k$ | Transportation of turbulent kinetic energy by diffusion, Pa/s |
| $D_\varepsilon$ | Transportation of dissipation of turbulent kinetic energy by diffusion, $Pa/s^2$ |
| $k$ | Turbulent kinetic energy, $m^2/s^2$ |
| $L_{CD}$ | Length of computational domain, m |
| $L_P$ | Length of pipe, m |
| $L_{Pt}$ | Protruding length of nozzle, m |
| $\dot{m}_{inlet}$ | Mass flow rate through the nozzle, kg/s |
| $\dot{m}_{suction}$ | Mass suction rate through the louvers, kg/s |
| $P$ | Pressure, Pa |
| Pr | Prandtl number |
| $Pr_t$ | Turbulent Prandtl number |
| $Re_n$ | Reynolds number based on nozzle ($\rho V_n D_n/\mu$) |
| $T$ | Temperature, K |
| $U$ | Velocity, m/s |
| $V_n$ | Velocity at nozzle exit, m/s |

***Greek Symbols***

| | |
|---|---|
| $\alpha$ | Thermal diffusivity, $m^2/s$ |
| $\varepsilon$ | Dissipation rate, $m^2/s^3$ |
| $\upsilon$ | Kinematic Viscosity, $m^2/s$ |
| $\rho$ | Density, $kg/m^3$ |
| $\mu$ | Shear viscosity, Pa.s |
| $\mu_t$ | Turbulent viscosity, Pa.s |
| $\sigma_k$ | Turbulent Prandtl number for $k$ |
| $\sigma_\varepsilon$ | Turbulent Prandtl number for $\varepsilon$ |
| $\phi$ | Scalar variable either k or ε |

**Subscripts**

| | |
|---|---|
| n | Nozzle |
| $\infty$ | Free stream |

traffic problems. The hot exhaust smoke coming from the vehicles with a high velocity may cause very serious problems specifically in respiratory systems of the two wheeler passengers and pedestrians. If the exhaust gases are cooled and the velocity was reduced before they are released, this problem can be controlled. The cooling and reduction in the velocity of the exhaust gases can be done by sucking fresh air from the atmosphere through louvers cut in the periphery of pipe

and also through the entrance opening without using any extra power from a pump. The high-speed gas coming out of the nozzle as shown in Fig. 1 creates a low pressure inside the pipe that is used to suck atmospheric air into the pipe to cool down the gas. Since the exhaust gases are hot, the material used for making the exhaust pipes should have high thermal resistance. If the exhaust gases are cooled, a cheaper material can be used to making the exhaust pipe thereby reducing the manufacturing cost of the vehicles on a large scale production. By achieving sufficient cooling of the exhaust gas, the rate of increase of local environmental temperature is controlled so that the adverse effect due to high-temperature vehicle emission can be avoided.

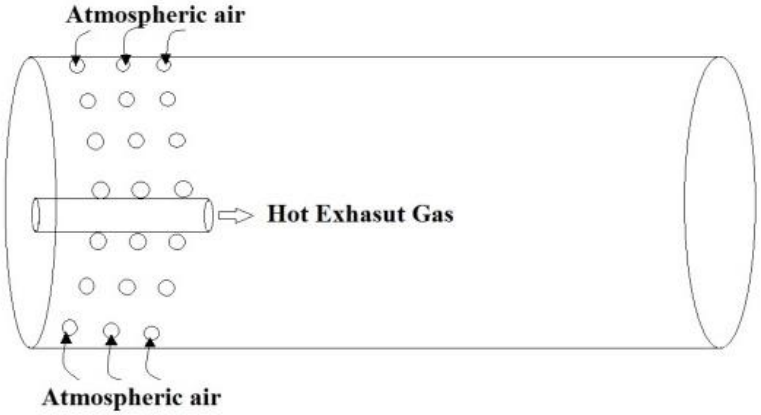


**Fig. 1. Schematic view of air suction into an open ended Louvered pipe due to high velocity air jet.**

Many research works have been performed by different investigators (both theoretically and experimentally) to study the flow characteristics and mass entrainment of air due to high-speed turbulent jets into cylindrical containers. Ricou and Spalding [1] described a new technique for measuring the axial mass flow rate formed by the turbulent jet when a gas is injected into a reservoir of stagnant air at uniform pressure. They found that the new technique for measuring the entrainment rate was applicable to jets of non-uniform density. They also found that the entrainment rate was increased by 30% when the injected gas burned in the jet. Hill [2] conducted an experiment to measure the local entrainment rate in the initial region of axi-symmetric turbulent air jets. He found that local entrainment rate was independent of nozzle Reynolds number for values more than $6\times10^4$ and strongly depended on the axial distance from the injection site. He concluded that the entrainment coefficient increased with axial distance in the initial region and became almost constant in the fully developed region. Han and Mungal [3] studied the entrainment of the turbulent jet in co-flow, with and without reaction by directly using Particle Image Velocimetry (PIV) for measurement. They found that the increase in co-flow speed reduced the entrainment for both reacting and non-reacting jets. They found that the entrainment in the near field of reacting jets was reduced by a factor of 2.5 due to the heat release effect. They also found that the effect of buoyancy increased the entrainment thereby compensating for the heat release effect in the reacting jet.

Mishra and Dash [4, 9] a conducted numerical investigation on air suction into louvers of funnel due to high-velocity air jet and concluded that air suction rate is enhanced with increase in louvers opening area but independent of the number of louvers per row. They also concluded that with total cross-sectional area and nozzle mass flow rate remaining constant, the use of multiple nozzles had no effect on air suction rate. They also found that to get maximum air suction effect, the protruding length of the nozzle was found to be around 0.5 m from the bottom wall of the funnel. The concluded that for an inverted frustum with a diameter ratio of 0.8 could suck maximum amount of air compared to a cylindrical funnel of the same volume.

Mishra et al. [5] also studied the effect of high-velocity isothermal air jet placed inside the funnel having different lengths of the protrusion and different funnel diameters. They concluded that for isothermal air suction the mass ingress into the funnel did not depend on the inclination of the funnel, but for low velocity and a high temperature of the nozzle fluid the mass ingress in to the funnel depends on the inclination of the funnel. They also found from the experimental and CFD computation that there existed an optimum funnel diameter and protrusion length of the nozzle for maximum air flow into the funnel. Singh et al. [6] used a finite element model to predict the level of entrainment and mixing in a confined turbulent jet of variable density. They achieved the turbulence closure by modified Brandt mixing length model. They found that the ratio of tube diameter and inlet jet diameter along with the ratio of free stream air density to the density of air at jet inlet condition were the main factors that influenced the entrainment and mixing. They also found that moving the jet away from the tube inlet increased the entrainment for short distances but reduced the entrainment for long distances. Barik et al. [7, 11] conducted an experimental and numerical investigation on air entrainment in infra-red suppression device. They concluded that the mass entrainment decreased, as the nozzle moved away from the bottom funnel. They found that the entrainment rate was reduced by 19.2% as the ratio of funnel overlap height, and nozzle diameter changed from 0 to 1.6. They also found new correlations for air entrainment into infra-red suppression device to predict the funnel exit temperature and mass entrainment into IRS device. Mishra et al. [8] also conducted a numerical investigation to find out an optimum design for maximum air entrainment into a mixing pipe. They found that the ratio of the forward length of mixing pipe and nozzle diameter had the highest effect on air entrainment rate. They concluded that the change in the ratio of forward mixing length and nozzle diameter from 5 to 20 changed the entrainment rate by 180%. Singh et al. [10] conducted an experimental investigation on entrainment characteristics of confined and semi-confined circular and noncircular jets. They found that non circular jets provided greater entrainment and mixing with ambient fluid than circular jets. They also found that entrainment ratio for all non-circular jets was more compared to a circular jet. They concluded that by shifting the location of jet, the entrainment was enhanced by 30%. Markatos [12] studied the flow phenomena involving turbulence in various practical applications. He aimed at using computational methods to provide details of the turbulent motion for engineering, environmental, bio medical, etc., processes. In this study, he found that the distance from the wall must be varied to fit the logarithmic wall law in the $k$-$\omega$ model. He also found that the $k$-$\varepsilon$ model was suitable to use because the $\varepsilon$ equation can be derived from N-S equation and the Brandt number for $\varepsilon$ had a

reasonable value which fit the experimental data for the spread of the various entities at locations far from walls.

Shokouhmand et al. [15] used finite element method to compute natural laminar unsteady convection heat transfer of an array of an isothermal oscillating cylinder. They have used 2-Dimensional incompressible Navier-Stokes equations coupled with the energy equation to analyse the heat transfer characteristics at various Rayleigh number. They reported that increasing Raleigh number and cylinder spacing augment the average Nusselt number for each cylinder as well as higher oscillating amplitude and frequency. They have also found that vortices appeared in the left and right area of the cylinders due to horizontal vibrations which reduced heat transfer from the cylinders. Shokouhmand et al. [16] investigated numerically two stationary vertical walls and two horizontal bottom, and top walls moving in opposite directions. Two vertical walls are heated uniformly and non-uniformly, and the two horizontal walls are adiabatic. They have used 2-Dimensional incompressible Navier-Stokes equation for various Reynolds number, Prandtl number and Grashof number. The governing equations, i.e., continuity, momentum and energy equations are discretized by using finite element method. The effect of uniform and non-uniform heating of vertical walls over a wide range of Reynolds number, Prandtl number and Grashof number on the thermal and fluid flow performance have been analysed.

Jafari et al. [17] in their numerical investigation used a control volume approach to survey a time-dependent two-dimensional mixed convection in a lid-driven cavity. They have utilized copper water Nano fluid with various Reynolds number, Grashof number, lid oscillation frequency and solid volume fraction. Their results revealed that higher average Nusselt number was observed by moving the lid in the negative direction as compared to moving the lid in the positive direction due to thermal boundary disturbance. They also found that at higher Reynolds number, the increment in lid frequency led to decrease in heat transfer.

The work found in the literature does not cite the use of CFD methods to determine the effect of various parameters on mass suction rate of air into a horizontal louvered pipe for a vehicle and hence to arrive at a specific design of the sucking pipe, which we plan to do in the present work. The study is carried out assuming exhaust pipe as the nozzle and hot air as the nozzle fluid and treated to be incompressible. We have attempted to match the existing experiment results of Singh et al. [10] with the present computational results.

## 2. Mathematical Formulation

A cylindrical pipe of diameter $D_P$ and length $L_P$ as shown in Fig. 2 was used to carry out the computational investigation. Air is allowed to enter the pipe through the louvers as well as the entrance face of the pipe. A nozzle of diameter $D_n$ having a protrusion length $L_{Pt}$ (into the pipe), is located at the centre of the entrance of the pipe to supply hot air. A cylindrical computational domain of diameter $D_{CD}$ (about 6 times of $D_P$) and length $L_{CD}$ (about 3 times of $L_P$) is placed around the pipe so that the boundary conditions can be applied on the computational domain for the suction takes near the louvers cut in the pipe. The louvers are made in a circular shape ($D_h$ = 0.03 m). A total of 12 louvers

are placed in each stack with a distance of 0.05 m being maintained between each stack. The flow field in the domain is computed by using three-dimensional, incompressible Navier-Stokes equations and a two equation based k-ε turbulence model with energy equation. The $Re_n$ (Reynolds number based on the nozzle diameter) varies from $2.4\times10^4$ to $2.6\times10^4$. The fluid used for simulation is air at 343 K with a mass flow rate of 0.02 kg/s at nozzle exit for all the cases and the flow treated to be incompressible. The values of mass flow rate and temperature of exhaust gas were calculated from the data available in the Internal Combustion engine laboratory of the institute. Steel (Density - 8030 kg/m$^3$, Specific Heat- 502.48 J/kg.K and Thermal Conductivity- 16.27 W/m-K) is taken as the solid material for all the walls defined for the present study.

### 2.1. Governing equations

The governing equations are used in the present analysis can be written as:

Continuity equation:

$$\frac{\partial}{\partial x_i}(\rho U_i) = 0 \tag{1}$$

Momentum equation:

$$\frac{D(\rho U_i)}{Dt} = -\frac{\partial p}{\partial x_i} + \frac{\partial}{\partial x_j}\left[\mu\left(\frac{\partial U_i}{\partial x_j} + \frac{\partial U_j}{\partial x_i}\right) - \rho\overline{u_i u_j}\right] \tag{2}$$

$$\frac{p}{\rho} = RT \tag{3}$$

The density $\rho$ is taken as the function of temperature according to the ideal gas law as per Eq. (3), while dynamic viscosity μ and thermal conductivity are kept constant.

Energy equation:

$$\frac{D(\rho T)}{Dt} = \frac{\partial}{\partial x_i}\left[\left(\frac{\mu}{\mathrm{Pr}} + \frac{\mu_t}{Pr_t}\right)\frac{\partial T}{\partial x_i}\right] \tag{4}$$

where, $Pr_t = 1$.

Turbulence kinetic energy *k:*

$$\frac{D}{Dt}(\rho k) = D_k + \rho P - \rho\varepsilon \tag{5}$$

where,

$$D_k = \frac{\partial}{\partial x_j}\left[\left(\mu + \frac{\mu_t}{\sigma_k}\right)\frac{\partial k}{\partial x_j}\right]$$

$\sigma_k = 1.0$

Dissipation rate of *k*:

$$\frac{D}{Dt}(\rho\varepsilon) = D_\varepsilon + C_{1\varepsilon}\rho P\frac{\varepsilon}{k} - C_{2\varepsilon}\rho\frac{\varepsilon^2}{k} \tag{6}$$

where,

$$D_\varepsilon = \frac{\partial}{\partial x_j}\left[\left(\mu + \frac{\mu_t}{\sigma_\varepsilon}\right)\frac{\partial\varepsilon}{\partial x_j}\right]$$

$C_{1\varepsilon} = 1.44$, $C_{2\varepsilon} = 1.92$, $\sigma_\varepsilon = 1.3$

$$\overline{u_i u_j} = \frac{2}{3}k\delta_{ij} - \nu_t\left(\frac{\partial U_i}{\partial x_j} + \frac{\partial U_j}{\partial x_i}\right) : \nu_t = C_\mu\frac{k^2}{\varepsilon} \tag{7}$$

where, $C_\mu = 0.09$

$$D_\phi = \frac{\partial}{\partial x_j}\left[\left(\mu + \frac{\mu_t}{\sigma_\phi}\right)\frac{\partial\phi}{\partial x_j}\right] \tag{8}$$

$$P = -\overline{u_i u_j}\frac{\partial U_i}{\partial x_j} \tag{9}$$

$\sigma_k$ and $\sigma_\varepsilon$ are the Prandtl numbers for k and ε. *R* is characteristic gas constant and is equal to 0.287 kJ/kg.K.

Although these constants are normally used for internal flows, but for the present case of mixed flow i.e. both for internal and external flow, we have not changed constants.

### 2.2. Boundary conditions

The boundary conditions for the open-ended louvered pipe can be seen from Fig. 2. The pipe and nozzle walls are solid and a no-slip boundary condition has been imposed. Pressure outlet boundary condition has been given to the top, side and bottom surface of the computational domain. Nozzle exit has been given velocity inlet and temperature boundary condition to supply hot air into the pipe. The velocity will be computed from the local pressure field to satisfy continuity at the pressure exit boundary while all the other variables like *T*, *k* and *ε* will be computed from zero gradient condition. The turbulent quantities, *k* and *ε* on the first near wall cell have been set from the equilibrium log law wall function as has been described by Jha and Dash [18, 19] and Jha et al. [20]. The turbulent intensity at the inlet of the nozzle has been set to 2% with the inlet velocity being known and the back flow turbulent intensity at all the pressure outlet boundaries have been set to 5%. If there is no back flow at a pressure outlet boundary, then the values of *k* and *ε* are computed from the zero gradient condition at that location.

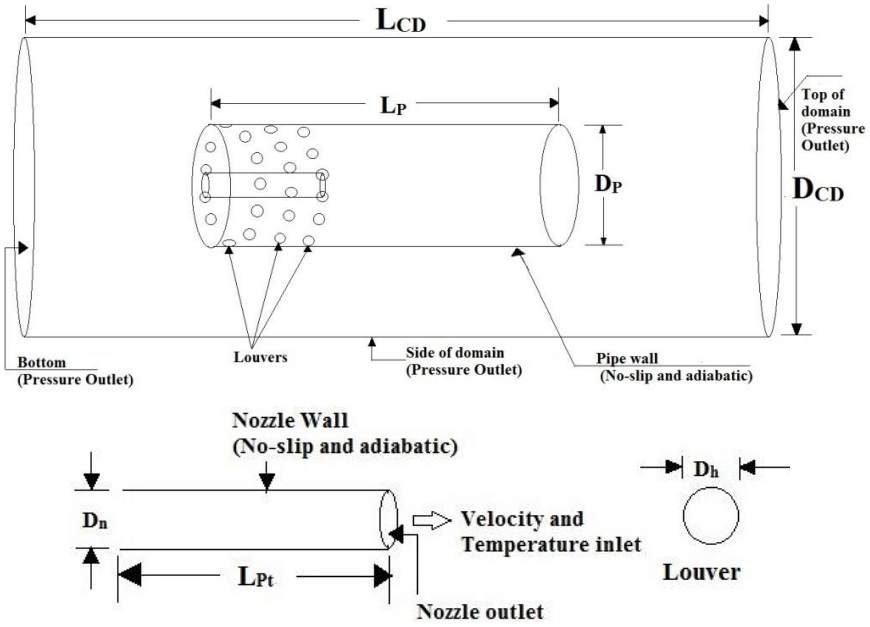


**Fig. 2. Schematic view of computational domain and the boundary conditions applied to it.**

## 3. Numerical Solution Procedure

The computational domain was discretized by using tetrahedral cells. The three-dimensional equations for mass, momentum and energy were discretized over control volume using finite volume technique to obtain a set of algebraic equations. These algebraic equations were solved by algebraic multi grid solver of using Fluent 14 by imposing proper boundary conditions stated earlier. First order upwind scheme was considered for discretized momentum and turbulent equations. The effect of domain size and number of grids has been discussed in detail separately in the results and discussions.

The SIMPLE algorithm with Standard scheme was used for the pressure-velocity coupling. Under relaxation factors of 0.3 for pressure, 0.7 for momentum, 0.8 for $k$ and $\varepsilon$ and 1 for temperature were used for the convergence of all variables. Fine grids were used at the nozzle entrance and louver openings to get better accuracy. Tetrahedral cells were used for the entire computational domain. Convergence criterion for the discretized equations for the whole field residual was set to $10^{-3}$ for all variables except for energy equation whereas for energy the residual level was kept at $10^{-6}$.

## 4. Results and Discussions

### 4.1. Comparison with other simulation results

We have attempted to match the entrainment of air into a confined jet in a cylindrical pipe where suction from the atmosphere was allowed only from

the bottom opening of the pipe close to the nozzle as shown in Fig. 3. The $Q_{suction}/Q_{inlet}$ obtained from numerical computation using *k-ε* turbulence model was compared with the existing experiment of Singh et al. [10] and Pritchard's relation [14] for confined jet (Fig. 3). It is seen form the plot the present CFD results are in good agreement with the analytic solution developed by Pritchard et al. [14] and experimental results of Singh et al. [10] with a maximum deviation of 8%. The radial profile of mean axial velocity of a wall-constraint jet can be seen from Fig. 5. The mean axial velocity *u(x, y)* is normalised by the centreline velocity *u(x, 0)* and the radial distance is scaled by the jet half width ($y_{0.5}$) which has been shown in detail in Fig.4. The jet half-width is defined as the transverse distance from the jet axis to the location where the mean axial velocity *u(x, y)* is half of the centreline value *u(x, 0)*. Singh et al. [10] and Becker et al. [13] proposed that if the velocity profile exhibits self-similarity, then the axial velocity profile will be reduced into a single curve. From Fig. 5, it can be seen that the results from the present CFD model for radial profiles are in good agreement with the experimental results from Singh et al. [10] and the empirical relation developed by Becker et al. [13]. The normalised velocity difference is clearly visualised towards the wall between the existing experimental measurement of Singh et al. [10] and present CFD. Actually the velocity towards the wall should be zero, but in the experiment it has shown a certain value because of error in the experiment.

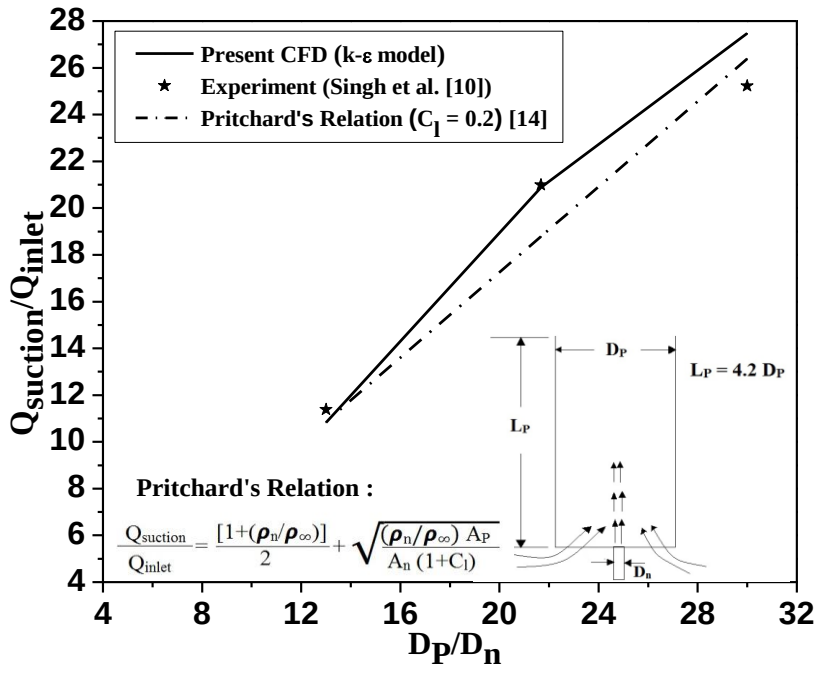


**Fig. 3. Entrainment ratio as a function of $D_P/D_n$: a comparison between present CFD with existing experiment [10] and Pritchard's relation [14].**

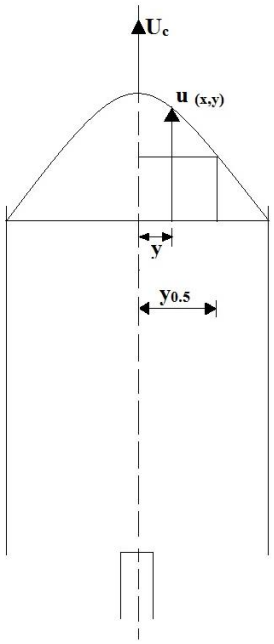


**Fig. 4. Schematic diagram showing the centreline velocity $U_c$ or $u(x, 0)$, mean axial velocity $u(x, y)$ and jet half width ($y_{0.5}$).**

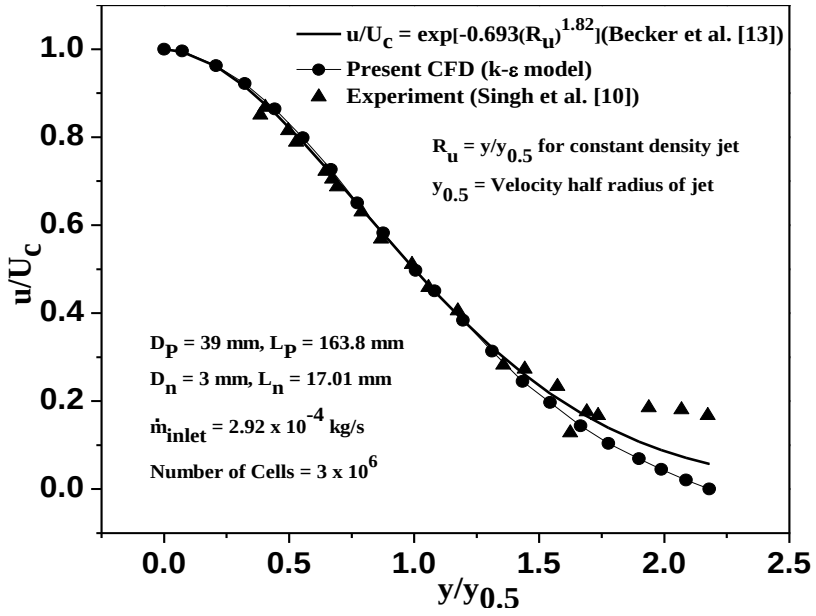


**Fig. 5. Radial profile of axial velocity of the existing experiment Singh et al. [10] compared with empirical correlation developed by Becker et al. [13] and with the present CFD.**

### 4.2. Effect of domain size on air suction rate

Three different sizes of computational domain (shown in Fig. 6) have been used to study the effect of the computational domain on the mass suction rate of air. For each case, the pipe diameter and length was fixed at 0.2 m and 1 m, while the diameter of the computational domain was varied from 4 to 8 times the pipe diameter and its length was varied from 2 to 4 times the pipe length. All the other parameters were kept constant which can be seen from Fig. 4. It can be clearly seen that the domain size has no appreciable effect on air suction rate. So the minimum size of the computational domain was selected as 3 m × 1.2 m ($L_{CD}$×$D_{CD}$) for the pipe of size 1 m × 0.2 m ($L_P$×$D_P$). Pressure outlet boundary condition was used on all the faces of the computational domain. The top surface of the computational domain allowed the air mass to flow out of the pipe, while other surfaces of the domain were used to allow the atmospheric air to come into the pipe from different locations on the pipe. Pressure outlet boundary was the only choice for the boundary condition for these types of cases.

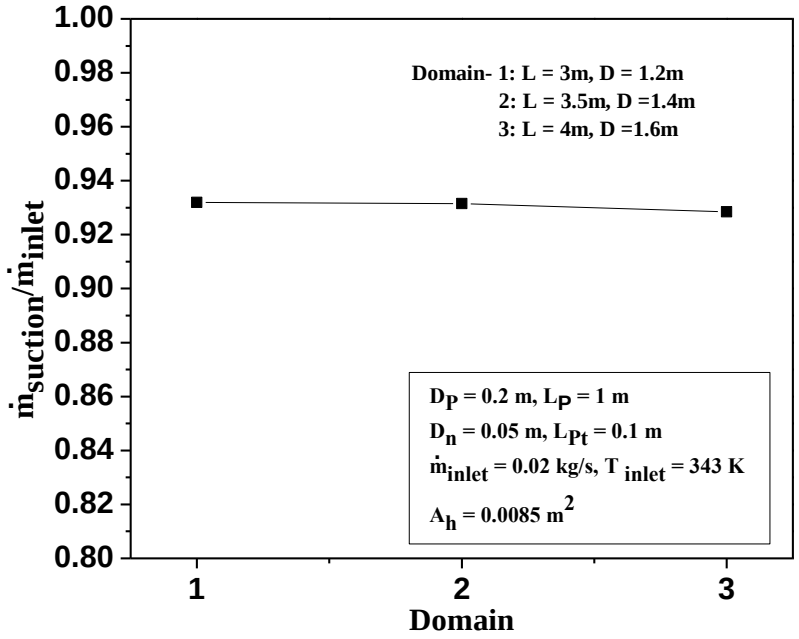


**Fig. 6. Effect of domain size on mass suction of air into the pipe.**

### 4.3. Effect of number of cells on air suction rate

The numerical investigation is started with a pipe diameter ($D_P$) and length ($L_P$) 0.2 m and 1 m respectively while the surrounding domain diameter ($D_{CD}$) and length ($L_{CD}$) of the were taken respectively as 1.2 m and 3 m. The nozzle diameter ($D_n$) and the protruding length ($L_{Pt}$) of the nozzle were taken as 0.05 m and 0.1 m respectively. The circumference of the pipe was cut with 12 numbers circular louvers per row ($D_h$ = 0.03 m, $A_h$ = 0.0085 $m^2$). The effect of cell numbers on mass suction rate were studied for louvers opening area of 0.0085 $m^2$. The

distance between each row was maintained at 0.05 m. The mass flow rate of air was maintained at 0.02 kg/s through the nozzle. This analysis was initiated by keeping all the other parameters constant as seen from Fig. 7. The cell numbers were varied from $1\times10^5$ to $2\times10^6$ and all cells are unstructured tetrahedral cells. The mass suction rate of air remained almost constant when the cell numbers are increased beyond $6\times10^5$. So $6\times10^5$ numbers of cells are used further computations. However when we change the configuration of pipe, we performed the grid test again before we report any results.

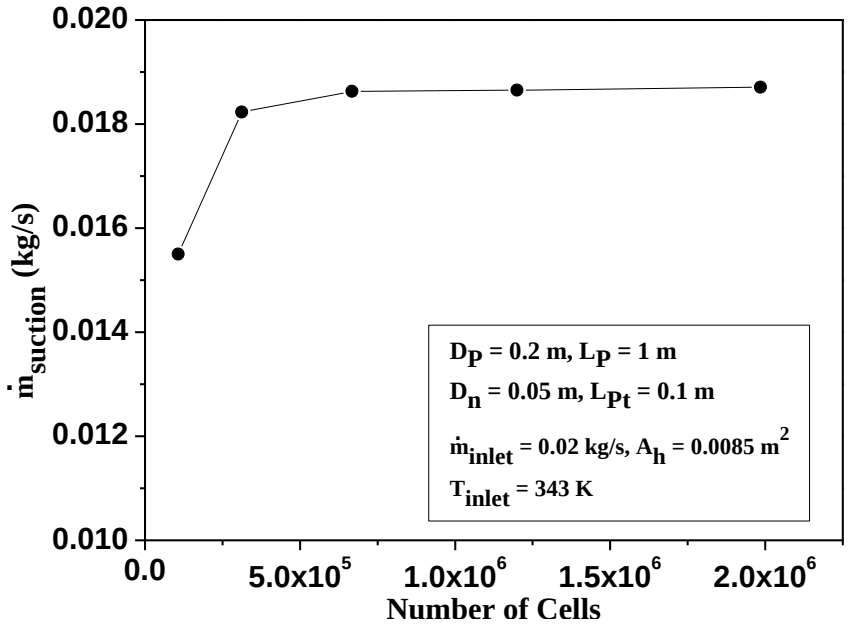


**Fig. 7. Effect of number of cells on air suction rate.**

## 4.4. Effect of total opening area on air suction rate

Figure 8 shows the effect of increasing total opening area as a function of pipe exit temperature and air suction rate. The simulations were carried out by keeping the area of the entrance face of the pipe constant at 0.0314 $m^2$ and taking the louver opening area as 0.0085 $m^2$, 0.017 $m^2$, 0.0255 $m^2$, 0.034 $m^2$, 0.0425 $m^2$, 0.051 $m^2$, 0.0595 $m^2$, 0.068 $m^2$ and 0.076 $m^2$. The nozzle mass flow rate was kept constant at 0.02 kg/s. The louver opening area was increased by adding rows of louvers placed symmetrically around the periphery. The distance between each row was maintained at 0.05 m. The nozzle diameter, nozzle protruding length, pipe diameter and pipe length and the area of the entrance face of the pipe were kept constant at 0.05 m, 0.1 m, 0.2 m, 1 m and 0.03142 $m^2$ respectively. From Fig. 6, it is clearly seen that by increasing the total opening area the air suction rate increases which decreases the pipe exit temperature. When the total opening area is increased by 2.5 times, the air suction rate is increased by 5%, which decreases the pipe exit temperature by 0.4 K. This clearly indicates the mass suction of air increased with the opening area.

A low pressure is created inside the pipe due to the high-velocity jet exit from the nozzle and as the surrounding pressure is high compared to the pipe inside pressure so air is rushed inside the pipe through the openings at the entrance as well as through the louvers and due to the mixing of the cold air the outlet temperature is dropped which is visualised from Fig. 6.

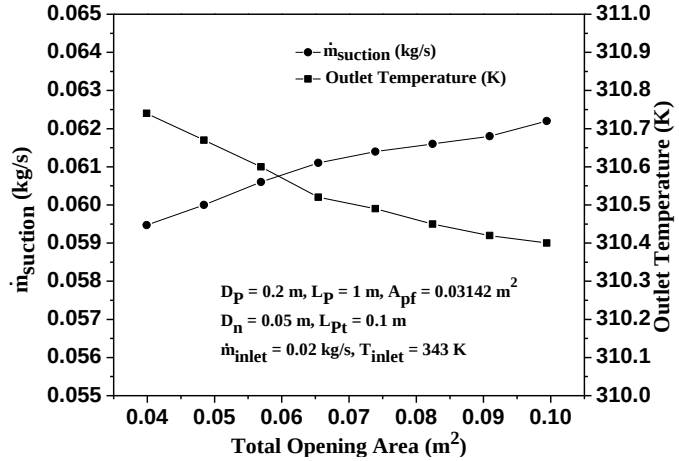


**Fig. 8. Effect of total opening area on air suction rate and pipe exit temperature.**

## 4.5. Effect of number of nozzles on air suction rate

Figure 9 shows the effect of the number of nozzles as the function of pipe exit temperature and mass ingress into the pipe. The numerical simulation was carried out for 1, 2, 4 and 6 nozzles. When single nozzle was used, it was located at the centre of the entrance face of the pipe and whereas in case multiple nozzles, they are located symmetrically at a pitch circle diameter of 0.1 m which can be seen from Fig.10. For single nozzle, the nozzle diameter was taken as 0.05 m. Total

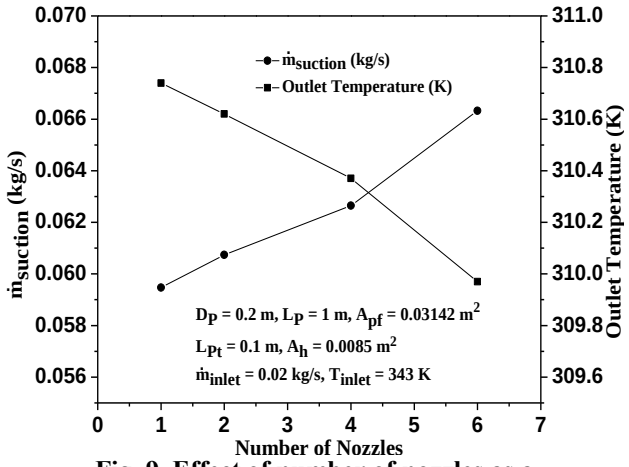


**Fig. 9. Effect of number of nozzles as a function of suction rate and pipe exit temperature.**

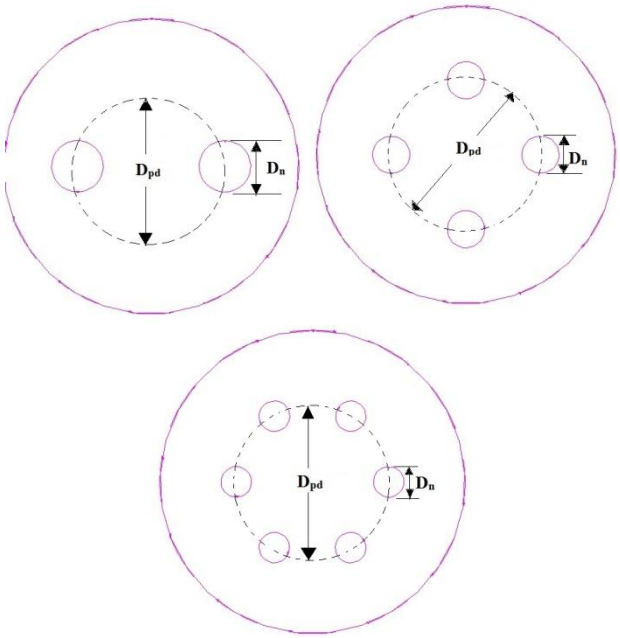


**Fig. 10. Multiple nozzles on pitch circle diameter.**

cross section area of the nozzle has been kept constant, at the diameters of 0.035 m, 0.025 m and 0.02 m for a nozzle number 2, 4 and 6. The numerical investigations were carried out by keeping the mass flow rate, louvers opening area, protruding length of the nozzle, pipe diameter and length along with the area of the entrance surface of the pipe constant at 0.02 kg/s, 0.0085 $m^2$, 0.1 m, 0.2 m, 1 m and 0.03142 $m^2$ respectively.

There was little change in air suction rate by increasing the nozzle number up to 4. But it was seen that when the nozzle number is increased to 6, the entrainment rate was increased to 1.11 times. As the number of nozzles increased, the low pressure is created uniformly inside the pipe and suction rate becoming more. Also, there is a possibility of better mixing of the hot and cold fluid inside the pipe hence the pipe exit temperature dropped sharply.

## 4.6. Effect of nozzle protrusion length on air suction rate

Figure 11 shows the effect of nozzle protruding length into the pipe on air suction rate as a function of pipe exit temperature. The pipe diameter, length, nozzle diameter, mass flow rate, louvers opening area and the inlet temperature of nozzle fluid along with the area of the entrance surface of the pipe were kept constant which can be seen from the plot. The air suction rate is decreased with increase in nozzle protrusion. So, the maximum air suction was obtained when the nozzle was at the entrance face of the pipe. When the nozzle is placed at the entrance of the pipe, the low pressure zone is created close to the entrance of the pipe, so the mass suction of air is highest at zero protrusion; therefore, the temperature is low at this location of the nozzle.

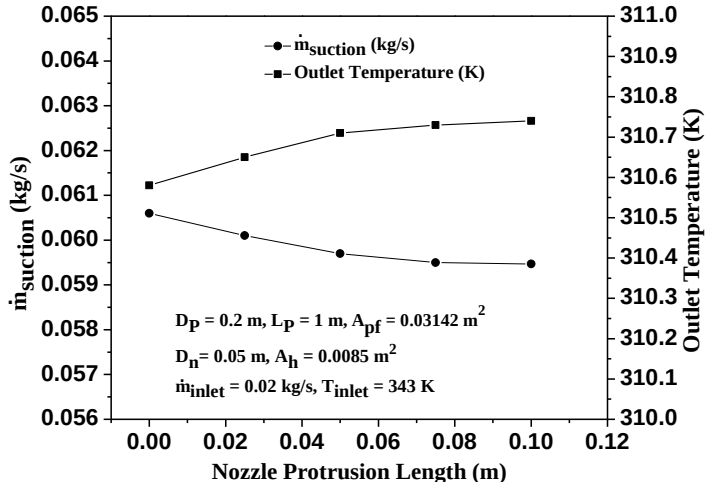


**Fig. 11. Effect of nozzle protrusion length as a function of air suction rate and pipe exit temperature.**

## 4.7. Effect of change in pipe diameter on air suction rate

Figure 12 shows the effect of the change in pipe diameter on air suction rate and pipe exit temperature. The size of the computational domain, louver opening area, pipe length, nozzle diameter, protrusion length mass flow rate and inlet temperature of nozzle fluid were kept constant which can be seen from the plot. The pipe diameter is increased from 0.15 m to 0.25 m. For a given mass flow rate through the nozzle, the amount of air sucked into pipe increases with the increase in pipe diameter. As the entrance face of the pipe is open to atmosphere, the increase in its area allows more air to be sucked into the pipe which thereby reduces the pipe exit temperature. So it is suggested that the increase in pipe diameter increases the mass suction of air. But from design constraint point of view the one cannot arbitrarily increase the pipe diameter of an exhaust system of a vehicle.

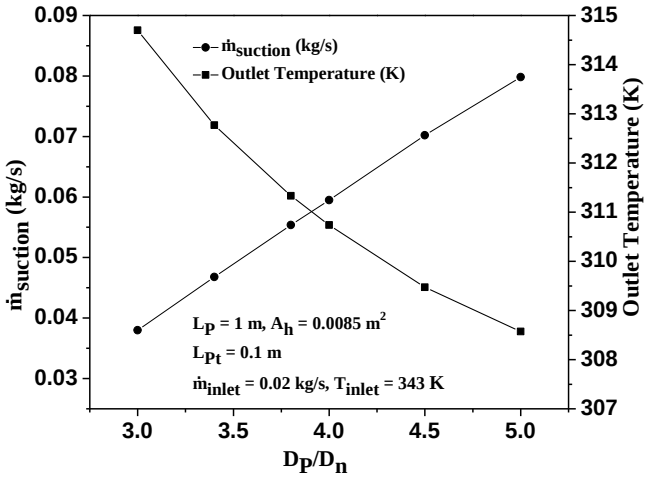


**Fig. 12. Effect of pipe diameter as a function of suction rate and pipe exit temperature.**

## 5. Conclusions

The numerical investigation of the parametric study of air suction rate through the louvers and entrance of a cylindrical pipe have been performed by solving the conservation equations of mass, momentum and energy with a two equation based k-ε turbulence model. The following conclusions can be drawn from the present numerical investigation:

- The mass suction rate of air is increased with the increase in total opening area which thereby decreases the exit temperature of the pipe.
- The mass suction of air into the pipe was increased by 1.11 times by using 6 nozzles as compared to a single nozzle.
- It is also found from the investigation the mass ingress of air is highest when the nozzle is placed at the entrance of the pipe.
- For a given nozzle mass flow rate and same lovers opening area, it was found that the mass suction of air into the pipe was increasing with pipe diameter.

## References

1. Ricou, F.P.; and Spalding, D.B. (1961). Measurements of entrainment by axisymmetrical turbulent jets. *Journal of Fluid Mechanics*, 11(1), 21-32.
2. Hill, B.J. (1972). Measurement of local entrainment rate in the initial region of axisymmetric turbulent air jets. *Journal of Fluid Mechanics*, 51(4), 773-779.
3. Han, D.; and Mungal, M.G. (2001). Direct measurement of entrainment in reacting/nonreacting turbulent jets. *Combustion and Flame*, 124(3), 370-386.
4. Mishra, D.P.; and Dash, S.K. (2010). Numerical investigation of air suction through louvers of a funnel due to high velocity air jet. *Computers & Fluids*, 39(9), 1597-1608.
5. Mishra, D.P.; Dash, S.K.; and Kishan, P.A. (2010). Isothermal jet suction through the lateral openings of cylindrical funnel. *Journal of Ship Research*, 54(4), 268-280.
6. Singh, G.S.; Sundarajan, T.; and Shet, U.S.P. (1999). Entrainment and mixing studies for a variable density confined jet. *Numerical Heat Transfer, Part A*, 35(2), 205-224.
7. Barik, A.K.; Dash, S.K.; and Guha, A. (2015). Experimental and numerical investigation of air entrainment into an infrared suppression device. *Applied Thermal Engineering*, 75, 33-44.
8. Mishra, D.P.; Samantaray, M.K.; and Dash, S.K. (2014) Maximum air entrainment into a mixing pipe through optimum design. *Ships and Offshore Structures*, 9(6), 605-611.
9. Mishra, D.P.; and Dash, S.K. (2011). Maximum air suction into a louvered funnel through optimum design. *Journal of Ship Research*, 55(1), 1-11.
10. Singh, G.S.; Sundarajan, T.; and Bhaskaran, K.A. (2003). Mixing and entrainment characteristics of circular and non-circular confined jets. *Journal of Fluid Engineering*, 125(5), 835-842.

11. Barik, A.K.; Dash, S.K.; and Guha, A. (2014). New correlations for prediction of air entrainment into an Infrared suppression (IRS) device. *Applied Ocean Research*, 47, 303-312.
12. Markatos, N.C. (1986). The mathematical modelling of turbulent flows. *Applied Mathematical Modelling*, 10, 190-220.
13. Becker, H.A.; Hottel, H.C.; and Williams, G.C. (1963). Mixing and flow in ducted turbulent jets. *In: 9th International Symposium on Combustion*. Pittsburg (PA): The Combustion Institute, 7-20.
14. Pritchard, R.; Guy, J.J.; and Conner, N. E. (1977). *Industrial gas utilization*. Bowker, New Providence, NJ.
15. Shokouhmand, H.; Noori Rahim Abadi, S. M. A.; and Jafari, A. (2011). The effect of the horizontal vibrations on natural heat transfer from an isothermal array of cylinders. *International Journal of Mechanics and Materials in Design*, 7(4), 313-326.
16. Shokouhmand, H.; Noori Rahim Abadi, S. M. A.; and Jafari, A. (2011). Finite element analysis of heat transfer within a square cavity with uniform and nonuniform boundary heating. *Heat Transfer Research*, 42(4), 337-358.
17. Jafari, A.; Rahimian, M.H.; and Saeedmanesh, A. (2013). An unsteady mixed convection in a driven cavity filled with nanofluids using an externally oscillating lid. *Journal of Electronics Cooling and Thermal Control*, 3(2), 58-73.
18. Jha, P.K.; and Dash, S.K. (2002). Effect of outlet positions and various turbulence models on mixing in a single and multi-strand tundish. *International Journal of Numerical Method for Heat and Fluid Flow*, 12(5), 560-584.
19. Jha, P.K.; and Dash, S.K., (2004). Employment of different turbulence models to the design of optimum steel flows in a tundish. *International Journal of Numerical Methods for Heat and Fluid*, 14(8), 953-979.
20. Jha, P.K.; Rajeev, R.; Mondal, S.S.; and Dash, S.K., (2003). Mixing in a tundish and a choice of turbulence model for its prediction. *International Journal of Numerical Methods for Heat and Fluid Flow*, 13(8), 964-996.